Original Article

Institution of MECHANICAL ENGINEERS
Journal of SYSTEMS AND CONTROL ENGINEERING

Proc IMechE Part I:
J Systems and Control Engineering
226(6) 742–760

DOI: 10.1177/0959651812440665
pii.sagepub.com
SAGE

Bond-graph-based fault detection and isolation for hybrid system models

Wolfgang Borutzky

Abstract

For the case when the abstraction of instantaneous state transitions is adopted, this paper proposes to start fault detection and isolation in an engineering system from a single time-invariant causality bond graph representation of a hybrid model. To that end, the paper picks up on a long-known proposal to model switching devices by a transformer modulated by a Boolean variable and a resistor in fixed conductance causality accounting for its ON resistance. Bond graph representations of hybrid system models developed in this way have been used so far mainly for the purpose of simulation. The paper shows that they can well constitute an approach to the bond-graph-based quantitative fault detection and isolation of *hybrid* models. Advantages are that the standard sequential causality assignment procedure can be a used without modification. A single set of analytical redundancy relations valid for all physically feasible system modes can be (automatically) derived from the bond graph. Stiff model equations due to small values of the ON resistance in the switch model may be avoided by symbolic reformulation of equations and letting the ON resistance of some switches tend to zero, turning them into ideal switches.

First, for two examples considered in the literature, it is shown that the approach proposed in this paper can produce the same analytical redundancy relations as were obtained from a hybrid bond graph with controlled junctions and the use of a sequential causality assignment procedure especially for fault detection and isolation purpose. Moreover, the usefulness of the proposed approach is illustrated in two case studies by its application to standard switching circuits extensively used in power electronic systems and by simulation of some fault scenarios. The approach, however, is not confined to the fault detection and isolation of such systems. Analytically validated simulation results obtained by means of the program Scilab give confidence in the approach.

Keywords

Hybrid models of engineering systems, FDI, ARRs, bond graphs, operation mode independent causalities, power electronic systems, averaged bond graph models

Date received: 29 October 2011; accepted: 20 January 2012

Introduction

Fast switching electronic devices such as diodes, transistors or thyristors in power electronics, hydraulic check valves, mechanical stops or clutches may give rise to the abstraction of instantaneous state changes. Often, this abstraction is justified and convenient as state transitions in such components or system parts happen to be much faster in comparison to the system dynamics of interest. As a result, models may encompass continuous time state changes and discrete events. Such models are usually termed hybrid models. As bond graph modelling is based on the exchange of energy between components, the methodology was initially used to capture continuous time phenomena. Extensions that also cover hybrid system models have been considered for a long time and various approaches have been reported in the literature. They may be categorised into those that aim at preserving an *invariant* computational causality assignment independent from system modes and those that allow for variable causalities.

As to bond graph models with static causalities, an early proposal has been to consider switching devices as non-ideal switches, to approximate their ON-OFF behaviour by a piecewise linear characteristic as displayed in Figure 1 with a set value e_{set} and a small ON resistance R_{on} and to represent switching devices modelled this

Bonn-Rhein-Sieg University of Applied Sciences, Germany

Corresponding author:
Wolfgang Borutzky, Bonn-Rhein-Sieg University of Applied Sciences,
?D-53754 Sankt Augustin, Germany.
Email: wolfgang.borutzky@h-brs.de

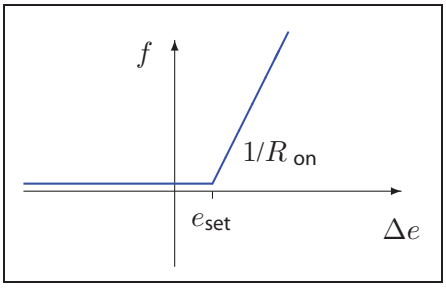

Figure 1. Piecewise linear approximation of the static characteristic of a switching device.

way by means of a modulated transformer (MTF): m controlled by a Boolean variable m in conjunction with a resistor R accounting for the small ON-resistance of the switch[1–3] as displayed in Figure 2. Clearly, the MTF and the resistor may be combined into a resistor with a variable time-dependent conductance $G(t)$: $= m^2(t)/R_{on} = m(t)/R_{on}$ and $m(t) \in \{0, 1\}\ \forall t \geqslant 0$ ($m = 0$: switch in OFF-mode, $m = 1$ switch in ON-mode).

Another way of capturing fast continuous state transitions is to model a switch by means of a resistor with a resistance or conductance $1/\epsilon$ ($\epsilon \in \mathbb{R}^+$) and to apply the singular perturbation method for separating the slow system dynamics from the fast physically insignificant ones.[4]

Other approaches also aiming at system mode *invariant* causalities have been the use of sinks of fixed causality switching off degrees of freedom,[5] or the use of a Petri net representing system modes and discrete changes between them along with a set of bond graphs with standard elements modelling the time-continuous behaviour in each identified physically feasible system mode.[6] Also, in order to account for ideal switching in a bond graph with time-invariant causalities, so-called switched power junctions (SPJs) have been introduced more recently.[7,8]

Bond graph representations of hybrid models allowing for *variable* causalities are based on the abstraction

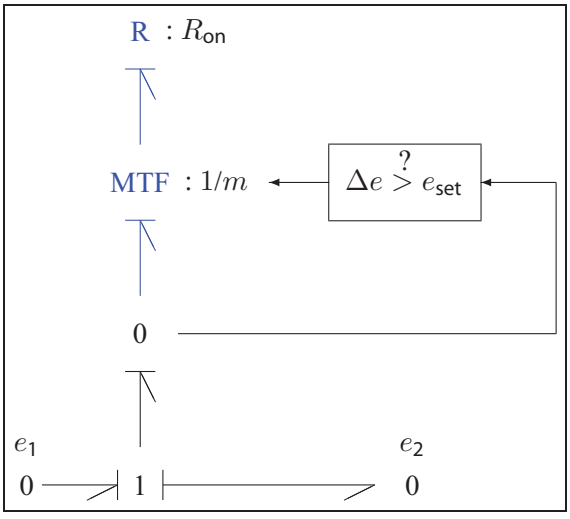

Figure 2. Modelling a switching device by means of a MTF and a resistor in conductance causality.

of ideal switches[9–12] (switched bond graphs), or use junctions controlled by a local automaton.[13,14] Bond graphs with such controlled junctions are usually called hybrid bond graphs (HBGs). Both approaches have their pros and cons (see e.g. Buisson et al.[4]). A survey of bond graph approaches to hybrid system modelling may be found in Borutzky.[15]

Beyond model development for the purpose of simulation, as early as 1995, publications, for example that of Tagina et al.,[16] have given rise to an increasing interest in bond graph model-based quantitative fault diagnosis resulting in remarkable achievements during recent years.[15,17–22] Due to the nature of bond graphs, the focus has been mainly on fault detection and isolation (FDI) in systems represented by time-continuous models. Narasimhan[23] uses HBGs for fault diagnosis in systems represented by hybrid models. As switching on or off controlled junctions entails at least a partial reassignment of causalities in a bond graph and affects the generation of explicitly formulated analytical redundancy relations (ARRs) as fault indicators, a modification of the sequential causality assignment procedure (SCAP) with respect to FDI has been recently proposed by Low et al.[24–26] In these references, the causal bond graph resulting from application of the modified assignment procedure is called a diagnostic hybrid bond graph.

The subject of this paper is bond-graph-based quantitative FDI in *hybrid* system models. Instead of using a variable causality approach, the paper aims at a bond graph representation with *invariant* causality from which a single set of ARRs can be derived that hold for all physically feasible operation modes. To that end, the early representation of a switch considered non-ideal by means of a MTF controlled by a Boolean variable in conjunction with a resistor is adopted. This approach offers the following advantages.

- The standard SCAP can be applied without modification. As a result, ports get time-invariant computational causalities.
- If nonlinearities permit the elimination of unknown variables from flow or effort balances derived from junctions, a single set of ARRs can be set up that hold for all system modes. Otherwise, a DAE system must be solved numerically in order to evaluate residual equations. In any case, neither model equations nor ARRs need to be reformulated after a switch state has changed.
- ARRs can be generated in the same way as for continuous-time system models. Existing software such as SYMBOLS[27] can be used to generate a set of ARRs which, however, is not unique.
- Equations derived from a bond graph may be symbolically reformulated in such a way that the small ON resistance may tend to zero turning switches into ideal switches and avoiding small time constants. That is, ideal switches may be considered the limit case of non-ideal switches. Avoiding stiff

equations is of interest in case an explicit formulation of ARRs is not possible so that the model equations need to be solved numerically in order to determine the residuals of ARRs.

The paper is organised in the following manner. The next section briefly revisits bond graph model-based quantitative fault detection and isolation. Subsequently, the derivation of ARRs from a bond graph of a hybrid model is considered. By means of two examples that have been considered in the literature it is shown that the approach proposed in this paper can produce the same ARRs that were obtained from a HBG with controlled junctions and the use of a SCAP especially modified for FDI purpose. Moreover, in the sections 'Boost converter' and 'Speed control of a buck converter-driven DC motor', the approach is illustrated by means of two elaborated case studies. The switching system examples under consideration are static converters with pairwise commutating switches as they are extensively used in power electronics. However, the representation of switching devices by means of a transformer with Boolean modulus and a resistor is not confined to electronically implemented switches and may be used for switching devices in other energy domains as well, e.g. for hydraulic check valves.

Bond graph model-based FDI

FDI is based on fault indicators. In a bond graph model-based approach to FDI, they can be provided by the sum of efforts or flows respectively at junctions. If nonlinear constitutive element equations of the model permit, unknown variables in these effort or flow balances can be replaced by inputs and known variables. That is, the result is constraint relations between known variables usually termed ARRs. The numerical evaluation of ARRs derived from a bond graph of a non-faulty system gives a residual that is either equal or close to zero due to numerical inaccuracies. If, however, values of the known variables in an ARR have been obtained by measurements of a real process or from another behavioural bond graph model accounting for possible faults in the process, then the residuals of ARRs are likely to be different from zero over time due to noise in measurement, to parameter uncertainties or due to the occurrence of faults. Noise in measurement can be suppressed by appropriate filtering before measured values are used for diagnosis. If the residuals of some ARRs exceed certain thresholds, then this event indicates that faults have happened in one or more system components. In order to avoid false alarms, thresholds should be adapted to system modes or at least carefully chosen.

As more than one system component usually contributes to an ARR, it is not clear in which component the indicated faults have occurred. The information of which components are involved in an ARR is called the signature of the residual. Residuals with different signature are called structurally independent. Their number is equal to the number of sensors added to a system.[22] However, the set of ARRs is not unique. The information of which system component contributes to which residual is usually expressed in a structural fault signature matrix (FSM) with entries 0 or 1 (0: component does not contribute to ARR; 1: fault in component affects ARR).[28] A diagonal submatrix of a FSM directly indicates faults that can be isolated, i.e. that can be uniquely attributed to a system component. If there are more fault candidates than residuals, i.e. the FSM is non-square, then depending on the pattern of nonzero entries in the non-square submatrix a fault candidate may be isolated under the single-fault hypothesis (only one fault at time) while not under the multiple simultaneous fault hypothesis.[19]

For isolation of *multiple simultaneous* faults from continuous-time models, parameter estimation by means of least-squares optimisation has been used.[19,29] Sensitivity analysis allows for assessing the severity of faults.

For systems with switching devices the structure of a bond graph is system mode dependent and so is the pattern of nonzero entries in a FSM reflecting the structure of ARRs derived from the bond graph. In other words, there is a FSM for each system mode. That is, isolation of faults by means of parameter estimation can be performed within the time span of a system mode using the set of ARRs of the current system mode. After a discrete change from one system mode to another the set of ARRs of the new system mode is to be used. To that end, the time points of the discrete mode changes must be located which can be done by using a DAE solver with root finding capability for computation of the model equations. A system mode is determined by a configuration of switch states. If the switch states are controlled by variables $m \in \{0, 1\}$ and if these variables are coefficients in the ARRs then the change from one set to another set of ARRs is achieved by just changing the values of the variables controlling the switch states.

To keep the presentation of the proposed bond-graph-based approach to FDI from hybrid system models easy to survey, in the following, the often-used single-fault hypothesis is adopted.

Off-line FDI

In the following, the proposed invariant causality bond graph approach to FDI from hybrid systems is presented in the context of off-line FDI. As in some publications of other authors, a behavioural model of a real system has been used instead of the system itself and this has been coupled to the invariant causality diagnostic bond graph of the hybrid model. An advantage of off-line FDI is that without any damage or risk all kinds of faults can be deliberately introduced into the behavioural model and their effect on the residuals of ARRs can be studied. In order to make the simulation even more realistic, outputs from the behavioural model could be superimposed with noise accounting

for sensor noise before they are fed into the diagnostic bond graph[22] so that they are closer to measurements from a real system. The resulting ARR residual values then should be averaged and possible pulses at switching times should be filtered in order to avoid misinterpretations leading to false alarms.

Robust FDI

As ARR residuals depend on parameters that may have actual values deviating from their nominal value or are varying with time, it is of interest to know how sensitive ARR residuals are to which parameters. A structural FSM only indicates which parameters affect which residual. Several bond graph approaches to sensitivity analysis of ARRs have been recently proposed in the literature[18,19,29] (see also Chapter 4 of Borutzky[17]).

Moreover, FDI should be robust with regard to sensor noise as well as modelling errors caused by parameter errors or by parameter variations but sensitive to system faults. One way to achieve robust FDI, known as the *passive approach*, is to let parameter uncertainties affect ARR residuals and to assess them in the decision-making process. Recent research using bond graphs in linear fractional transformation (LFT) form has demonstrated that ARRs can be derived in a form with a nominal and an uncertain part. The latter accounts for parameter uncertainties and gives rise to the definition of thresholds for non-faulty operation (Chapters 3 and 7 of Borutzky[17]; see also Djeziri et al.[20]). In order to avoid missing or false alarms, residual thresholds should be neither too narrow nor too large. Borutzky[30] shows that the approach presented in this paper can be combined with *incremental* bond graphs (Borutzky and Granda,[31] and Chapter 4 of Borutzky[17]), to derive system mode dependent adaptive thresholds for ARRs that account for parameter uncertainties.

Another approach to robust FDI, known as the *active* approach, is to decouple the effect of modelling errors and disturbances from the residual signals.[32,33] If modelling errors are parameter uncertainties they may be decoupled and treated as structured uncertainties. Bond graph modelling of structured parameter uncertainties has been presented by Kam and Dauphin-Tanguy.[34]

Finally, FDI should also be robust with regard to input disturbances. A bond graph approach to robust FDI in the presence of input uncertainties assumed to be additive and bounded has been recently presented by Touati et al.[35] In the more general case of non-classified disturbances robust residuals can be obtained by application of statistical methods to data obtained from measurements or simulation.[36]

ARRs from bond graphs of hybrid system models

In this paper, FDI starts from bond graphs of hybrid models in which switches have been represented by a transformer modulated by a Boolean variable and a resistor in conductance causality as has been initially proposed by Ducreux et al. for bond graph modelling of power electronic circuits.[2] That is, the SCAP can be applied without modification. The result is a bond graph of a hybrid model with *static* causalities that holds for all physically feasible combinations of switch states. From such a bond graph of a hybrid model, ARRs can be derived in the same way as from a bond graph of a continuous time model. Moreover, this step can be performed using existing software such as SYMBOLS.[27]

By contrast, in Low et al.,[25] bond graphs of hybrid system models make use of controlled junctions. Thus, computational causalities become variable. In ON-mode, a controlled junction is identical with a standard bond graph junction. In OFF-mode, it may be replaced by a zero-value source. Its type depends on the type of junction[14] (see Figure 3). As controlled junctions switch on and off parts of the bond graph, at least a partial reassignment of computational causalities becomes necessary.[37,38] For instance, for a standard 0-junction, causality rules require that one of the n attached bond imposes an effort on the junction and that this received information is passed on by the remaining n 1 bonds. In contrast, all bonds attached to a controlled 0-junction impose an effort on the ports of adjacent elements if the junction is in OFF-mode (Figure 3). This change in causality after a switch has changed its state is to be propagated into the bond graph and may entail that some storage ports change from integral to derivative causality so that the dimension of the state vector is reduced.

Aiming at a set of ARRs that holds for all system modes, Low and his co-workers study the computational causality effects controlled junctions have on adjacent parts of the bond graph under alternative causality assignments and propose a modification of the SCAP especially suited for FDI by introducing preferred causalities for controlled junctions.[26] They term the bond graph with causalities assigned according to this modified procedure the diagnostic hybrid bond graph (DHBG) and denote ARRs derived from the DHBG as global ARRs (GARRs). This procedure is applied by Low et al.[25] to a network example. In the following, this example is adopted to show that the *invariant* causality bond graph approach to FDI proposed in this paper leads to the same ARRs as given by Low et al.[25]

Derivation of ARRs from an electrical network with a switching transistor

Figure 4 displays the circuit diagram given by Low et al.[25] Figure 5 shows an associated invariant causality

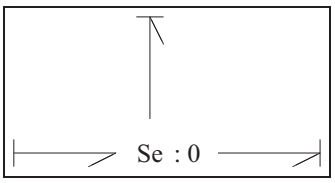

Figure 3. Controlled 0-junction in OFF-mode.

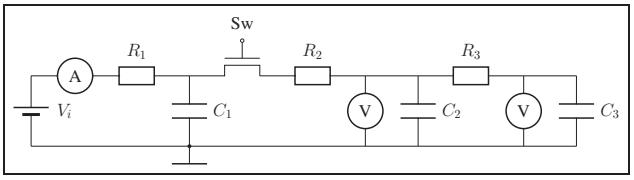

Figure 4. Network with a switch (Low et al.[25])

bond graph with Boolean-controlled MTFs. As can be seen from the bond graph in Figure 5, detector causalities have been inverted and *derivative* causality has been assigned to energy stores as proposed by Samantaray et al.[19] although this is not necessary for the derivation of ARRs expressed in terms of the derivatives of energy storage variables instead of their integral. For such bond graphs, Samantaray et al. have termed the notion diagnostic bond graph (DBG). DBG models are useful in online FDI when measurements from a real process are fed into a DBG model. Preferred derivative causality at storage ports avoids the need for initial values that are unknown. A disadvantage is that numerical differentiation of measured inputs needs to be carried out. The auxiliary capacitor $C : C_a$ in integral causality with a small capacitance C_a has been added to resolve the causal conflict at junction 0_2. In its constitutive relation solved for its current, C_a is considered small so that the current vanishes. In the formulation of equations, the parameter of an auxiliary storage element used for resolving a causality conflict at a junction is set to zero. That is, the auxiliary storage elements will not lead to a set of stiff model equations with regard to simulation performed for a numerical evaluation of the residuals of ARRs.

For comparison, Figure 6 reproduces the hybrid bond graph given by Low et al.[25] As storage elements are assigned preferred derivative causality, the notion DHBG is used by Low et al.[25] However, note that in contrast to DBGs as introduced by Samantaray, detector causalities in DHBGs are not inverted as shown in Figure 6. That is, the adjective *diagnostic* is slightly differently used in the literature. This paper follows the notion introduced by Samantaray meaning a bond

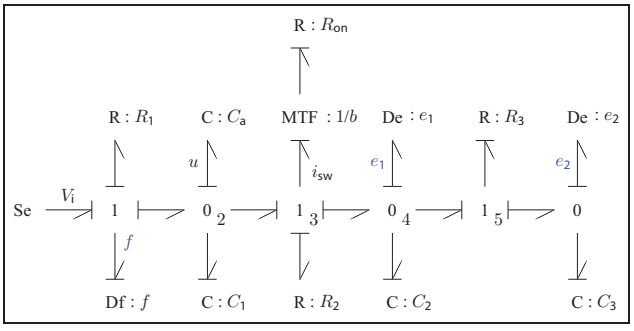

Figure 5. Invariant causality diagnostic bond graph with Boolean-controlled MTF of the network in Figure 4.

graph with storage elements in preferred derivative causality and detectors with inverted causality. In the DHBG of Figure 6, junction 1_3 is a *controlled* junction accounting for the connection and disconnection of circuit nodes by the pass transistor modelled as a switch. The resistor $R : R_{p2}$ is an artificial resistor resolving the causal conflict at junction 0_4 similar to the auxiliary capacitor $C : C_a$ in the bond graph of Figure 5.

ARRs are derived by Low et al.[25] from the junctions $0_2, 0_4$, and 1_5. In general, ARRs are obtained from the balance equation of those junctions to which a detector has been attached that represent a real sensor. According to the choice of junctions made by Low et al.,[25] summation of flows at junction 0_2 of the invariant causality bond graph in Figure 5 yields for the residual r_1

$$r_1 = f \quad C_1\dot{u} \quad i_{sw} \quad C_a\dot{u} \tag{1}\leftarrow$$

As C_a is assumed to be very small, the term $C_a\dot{u}$ can be neglected in equation (1). Due to the conductance causality of the ON resistance $R : R_{on}$ the constitutive relation of the switch takes the form

$$i_{sw} = \frac{b^2}{R_{on} + b^2R_2}(u \quad e_1) \tag{2}\leftarrow$$

where $b \in \{0, 1\}$. Finally, the voltage u is determined from the sum of efforts at the left 1-junction

$$u = V_i \quad R_1 f \tag{3}\leftarrow$$

As a result, the ARR for residual r_1 reads

$$r_1 = f \quad C_1\frac{d}{dt}(V_i \quad R_1 f) \quad \frac{b^2}{R_{on} + b^2R_2}(V_i \quad R_1 f \quad e_1) \tag{4}\leftarrow$$

As the right-hand side expression includes the coefficient b that accounts for the switch state, this ARR holds for all system modes. According to Low et al.,[25] it is a GARR.

Likewise, summation of flows at junction 0_4 and of efforts at junction 1_5 respectively and elimination of unknown variables following causal paths in the bond graph gives the ARRs

$$r_2 = i_{sw} \quad C_2\dot{e}_1 \quad C_3\dot{e}_2 \tag{5}\leftarrow$$

$$r_3 = e_1 \quad R_3C_3\dot{e}_2 \quad e_2 \tag{6}\leftarrow$$

These results obtained from the invariant causality bond graph in Figure 5 with modulated transformers

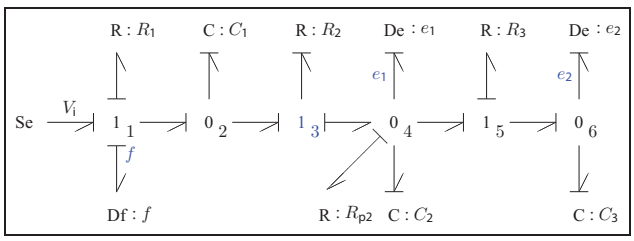

Figure 6. DHBG of the network according to Low et al.[25]

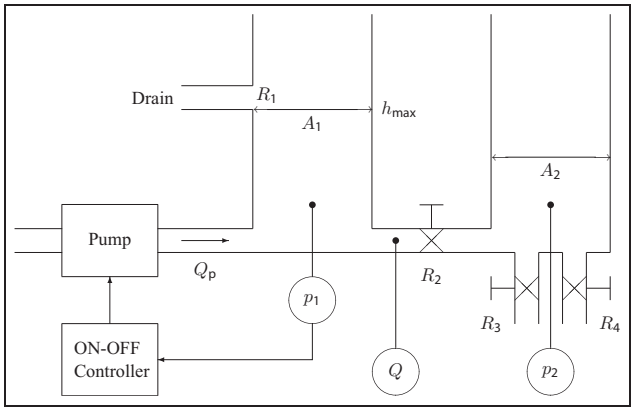

Figure 7. Two-tank system (Low et al.[24])

instead of controlled junctions are identical to the ones derived from the variable causality DHBG in Low et al.[25] if R_{on} is neglected in the ON mode of the switch. That is, the switches are considered ideal.

Furthermore, Low et al.[24] explain the approach to FDI from hybrid system models based on hybrid bond graphs and a modification of the SCAP suited for FDI by considering a slight modification of the well known hydraulic two-tank system. In this system, the feeding pump is controlled by an ON–OFF controller to ensure that the fluid level in the tank connected to the pump does not exceed a certain level. In addition, this tank has got a drain to prevent an overflow in case the controller fails.

The following section briefly shows that for this example as well the invariant causality bond graph approach to FDI proposed in this paper leads to the same ARRs.

Derivations of ARRs from a hybrid model of a controlled hydraulic two-tank system

The system schematic has been reproduced in Figure 7. Figure 8 displays an invariant causality diagnostic bond graph with Boolean-controlled MTFs of that system where $b_1, b_2 \in \{0, 1\}$, $p_D := \rho g h_{max}$ and ρ denotes a constant value for the fluid density.

Adding flows at junction 0_1, 1_1 and 0_2 gives the following residuals

$$0_1: \quad r_1 = b_1 Q_p \quad C_1\dot{p}_1 \quad b_2 k_1 \sqrt{b_2(p_1 \quad p_D)} \quad Q \qquad (7)\leftarrow$$

$$1_1: \quad r_2 = p_1 \quad p_2 \quad k_2 \text{sign}(p_1 \quad p_2)\sqrt{|p_1 \quad p_2|} \qquad (8)\leftarrow$$

$$0_2: \quad r_3 = Q \quad C_2\dot{p}_2 \quad k_3\sqrt{\overleftarrow{p_2}} \quad k_4\sqrt{\overleftarrow{p_2}} \qquad (9)\leftarrow$$

where k_1, k_2, k_3, and k_4 are constants, $b_2 = 0$ for $p_1 \leqslant p_D$ and $b_2 = 1$ for $p_1 > p_D$ (overflow) and $b_1 = 1$ b_2.

Finally, writing the controller equation in implicit form gives another ARR. For simplicity, it is assumed that the ON–OFF controller operates without any fault so that this ARR can be omitted.

Structural FSMs

The structural information in the above ARRs is captured by the structural fault signature matrix $\mathbf{S} = (s_{ij})$ shown in Table 1. An entry with the value one in the additional column with the heading D_b indicates that the fault in that row can be *detected*, while a zero-entry in the second additional column with the heading I_b denotes that the fault cannot be *isolated*. The *i*th fault can be detected if at least one residual is sensitive to it, i.e. if there is an index *j* such that $s_{ij} = 1$. A fault with the index *i* can be isolated if it can be detected and if in addition the pattern of entries in the *i*th row called *fault signature* is different from that of all other rows.

The last three rows may be omitted if non-faulty sensors are assumed. Clearly, a failure in the controlled pump affecting the volume flow Q_p it delivers and a failure in the drain can only be detected when these components are active. As there are two Boolean moduli b_1 and b_2, four system modes exist. Since the Boolean moduli are entries in the FSM, the latter holds for all operating modes.

In the following, the proposed *invariant* causality bond graph approach to FDI is applied in two case studies. For illustration, electronic converters with pairwise switching devices are considered as example systems as they are extensively used in power electronics.

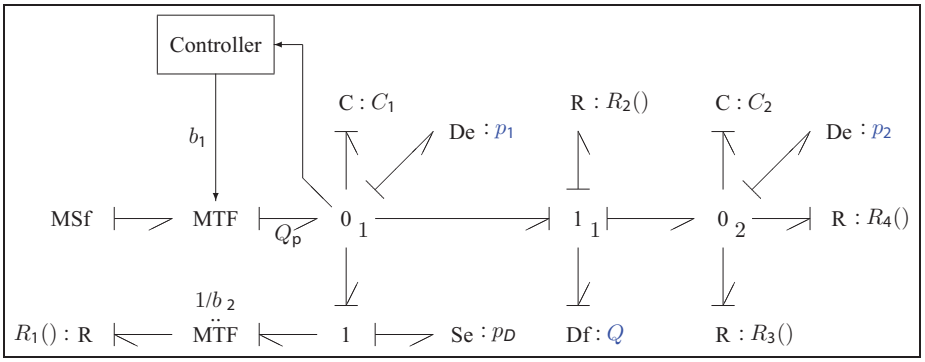

Figure 8. Invariant causality diagnostic bond graph with Boolean-controlled MTFs of the two-tank system.

Table 1. Structural FSM of the two tank system with sensors De : p_1, De : p_2 and Df : Q.

Component	Parameter	r_1	r_2	r_3	D_b	I_b
Controlled pump	b_1	b_1	0	0	b_1	0
Tank 1	C_1	1	0	0	1	0
Tank 2	C_2	0	0	1	1	0
Drain	k_1	b_2	0	0	b_2	0
Valve 1	k_2	0	1	0	1	1
Valve 2	k_3	0	0	1	1	0
Valve 3	k_4	0	0	1	1	0
Sensor of p_1	p_1	1	1	0	1	1
Sensor of p_2	p_2	0	1	1	1	1
Sensor of Q	Q	1	0	1	1	1

The proposed approach, however, is not confined to such systems. The considered fault scenarios assume abrupt faults because their effect on ARR residuals is usually more distinct than the one of incipient faults.

First, a classical boost converter with a load resistor is considered.

Boost converter

Figure 9 shows the schematic of a boost converter circuit with a load resistor. Figure 10 depicts a bond graph model in which the MOSFET transistor and the diode have been captured by a Boolean-controlled modulated transformer in conjunction with a resistor. The latter accounts for the ON-resistance of the switching devices. The integral causality of the inductor $I : L$ and the conductance causality of the submodel for the switching devices leaves the causality at junction 0_1 undetermined. To resolve the causal conflict, an auxiliary capacitor $C : C_a$ has been added. As its capacitance C_a is considered very small, the current $i_a := C_a \dot{u}$ is neglected. Accordingly, the following two state equations can be derived from the bond graph in Figure 10

$$L\frac{di_L}{dt} = E \quad R_L i_L \quad u \tag{10a}\leftarrow$$

$$C\frac{duC}{dt} = i_D \quad \frac{1}{R}u_C \tag{10b}\leftarrow$$

where

$$\frac{m_1^2}{R_{sw}} + \frac{m_2^2}{R_D}\ u = i_L + \frac{m_2^2}{R_D}u_C \tag{11a}\leftarrow$$

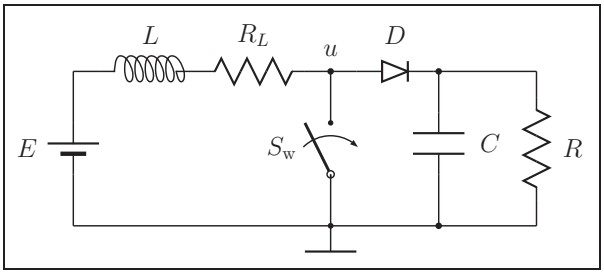

Figure 9. Boost converter circuit schematic.

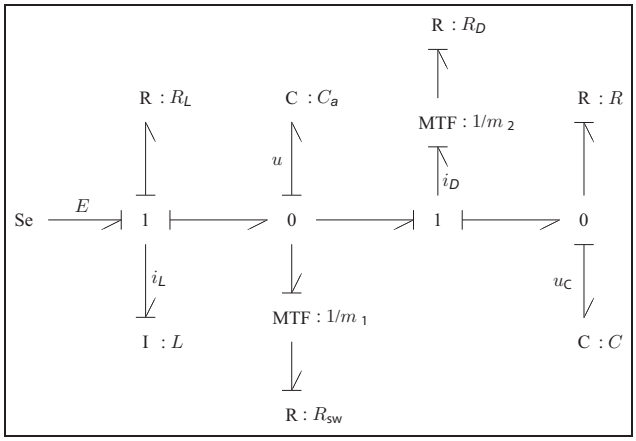

Figure 10. Bond graph model of the boost converter circuit.

$$i_D = \frac{m_2^2}{R_D}(u \quad u_C) \tag{11b}\leftarrow$$

$$m_2(t) := 1 \quad m_1(t) \text{ and } m_1(t) \in \{0, 1\} \quad \forall t \geqslant 0.$$

For $R_{sw} = R_D = R_{on}$ the state equations reduce to

$$\begin{matrix} L & 0 \\ 0 & C \end{matrix} \begin{matrix} \frac{d}{dt} & i_L \\ & u_C \end{matrix} = \begin{matrix} (R_L + R_{on}) & m_2(t) \\ m_2(t) & \frac{1}{R} \end{matrix} \begin{matrix} i_L \\ u_C \end{matrix} + \begin{matrix} 1 \\ 0 \end{matrix} [E](\tag{12}\leftarrow$$

According to equation (12), the boost converter can be represented by the alternative bond graph in Figure 11.

Average models

For power electronic systems often averaged models are considered. Their numerical evaluation may be faster and results can be more easily checked. Average bond graph models of power converters have been presented by Allard et al.[39] and Garcia-Gomez et al.[40]

Taking the average of the expressions on both sides of the second state equations (12) over the switching time period T_s, i.e.

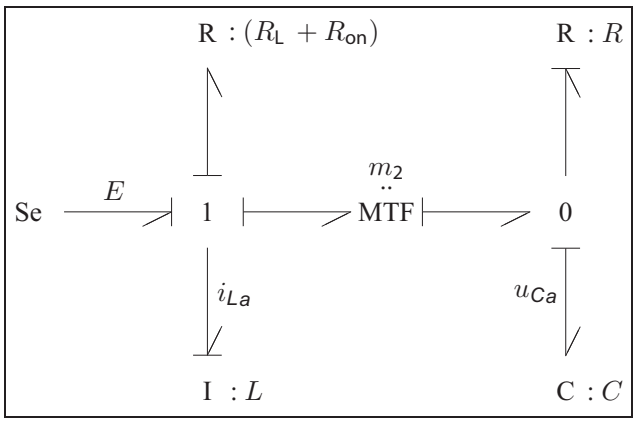

Figure 11. Alternative bond graph model of the boost converter.

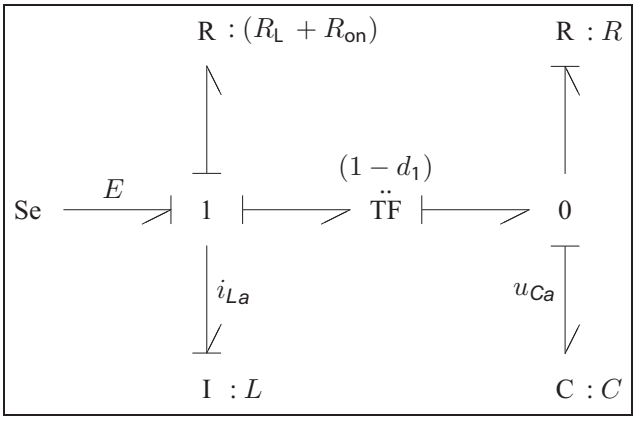

Figure 12. Bond graph of the averaged model of the boost converter circuit.

$$\frac{1}{T_s}\int_0^{T_s} C\dot{u}_C dt = \frac{1}{T_s}\int_0^{T_s} (1 - m_1(t))i_L dt - \frac{1}{T_s}\int_0^{T_s} \frac{1}{R}u_C dt \quad (13)$$

leads to

$$C\dot{u}_{C_a} = (1 - d_1)i_{La} - \frac{1}{R}u_{Ca} \quad (14)$$

where the subscript a denotes averaged variables.

Hence, the state equations of the averaged model read

$$\begin{bmatrix} L & 0 \\ 0 & C \end{bmatrix} \frac{d}{dt}\begin{bmatrix} i_{La} \\ u_{Ca} \end{bmatrix} = \begin{bmatrix} -(R_L + R_{\text{on}}) & -(1-d_1) \\ (1-d_1) & -\frac{1}{R} \end{bmatrix} \begin{bmatrix} i_{La} \\ u_{Ca} \end{bmatrix} + \begin{bmatrix} 1 \\ 0 \end{bmatrix} [E] \quad (15)$$

where t_{on} denotes the duration the switch is on, T_s the switching time period, and $d_1 := t_{\text{on}}/T_s$ the duty ratio. The averaged model of the boost converter is represented by the bond graph in Figure 12.

Fault scenario 1: temporary change of the duty ratio d_1

Simulation of the system. Given the parameters in Table 2 with values adopted from Umarikar[7] and assuming that for the time period [0.04 s, 0.06 s] the value of the duty ratio d_1 drops to the value 0.35, a simulation run reveals for the inductor current i_L and the capacitor voltage u_C the time histories depicted in Figures 13 and 14 respectively. The time evolution of their mean values i_{L_a} and i_{C_a} respectively are also plotted in these figures. They have been obtained by computing the average bond graph model in Figure 12.

Neglecting R_{on}, the steady-state values of the averaged inductor current $i_{La}(t \to \infty) = 7.44\,A$ and the averaged capacitor voltage $u_{Ca}(t \to \infty) = 20.47\,V$ are easily obtained from equation (15) in accordance with the simulation results.

Table 2. Parameters of the boost converter circuit.

Parameter	Value	Units	Meaning
E	12.0	V	Voltage supply
L	1.0	mH	Inductance
R_L	0.1	Ω	Resistance of the coil
C	500	μF	Capacitance
R	5.0	Ω	Load resistance
T_s	10^{-3}	s	Switching time period
d_1	0.45	–	Duty ratio

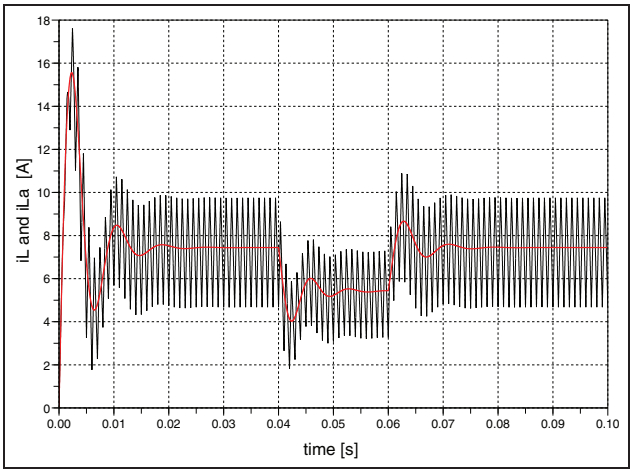

Figure 13. Time evolution of the inductor current i_L and its mean value i_{L_a} due to a reduced duty ratio during the interval [0.04 s, 0.06 s].

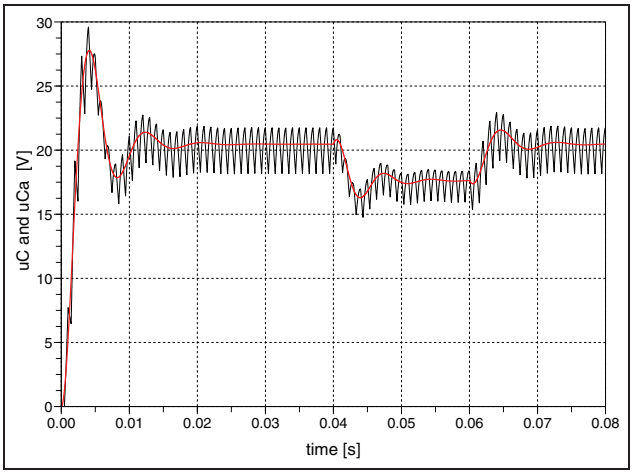

Figure 14. Time evolution of the capacitor voltage u_C and its mean value u_{C_a} due to a reduced duty ratio during the interval [0.04 s, 0.06 s].

Numerical computation of ARRs. It is assumed that the inductor current i_L and the voltage drop across the capacitor u_C are measured and, therefore, are known. Accordingly, their detectors in the diagnostic bond graph (Figure 15) have inverted causalities. Given $R_{\text{sw}} = R_D = R_{\text{on}}$, the following two ARRs can be derived from the diagnostic bond graph in Figure 15

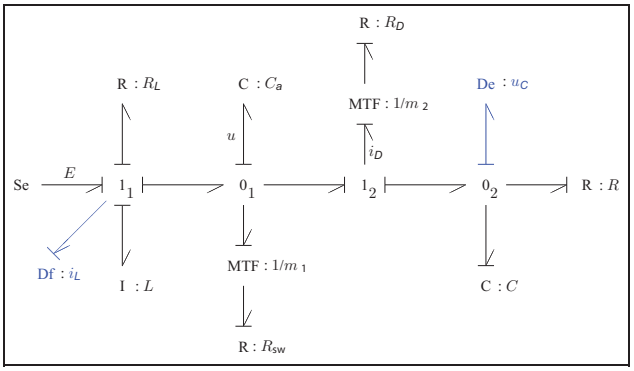

Figure 15. Diagnostic invariant causality bond graph of the boost converter circuit.

$$1_1: \quad r_1 = \quad (R_L + R_{on})i_L \quad m_2 u_C \quad L\frac{di_L}{dt} + E$$

$$= \quad (R_L + R_{on})i_L \quad (1 \quad m_1)u_C \quad L\frac{di_L}{dt} + E \qquad (16)\leftarrow$$

$$0_2: \quad r_2 = m_2 i_L \quad C\frac{du_C}{dt} \quad \frac{1}{R}u_C$$

$$= (1 \quad m_1)i_L \quad C\frac{du_C}{dt} \quad \frac{1}{R}u_C \qquad (17)\leftarrow$$

Table 3 shows the corresponding structural FSM. If it is assumed that the sensors are non-faulty then their rows could be omitted. As can been seen from the fault signature matrix, if the time history of both residuals deviate from zero in a given time interval, then this is an indicator for a change in the duty ratio d_1.

The time history of the residuals can be computed following an approach presented by the author.[18] A bond graph model of a non-faulty process is coupled to a bond graph model of the process subject to a fault by means of residual sinks. The latter impose a power variable onto the model of the non-faulty process forcing it to adapt to the faulty process behaviour. The outputs of the residual sinks are the residuals to be determined. The upper part of the bond graph in Figure 16 shows an average bond graph model of the non-faulty boost converter coupled by residual sinks rSe and rSf respectively to an average bond graph model of the boost converter with a disturbed duty ratio $\tilde{d}_1$ in the lower part of

Table 3. Structural FSM of the boost converter with sensors Df : i_L and De : u_C.

Component	Parameter/output	r_1	r_2	D_b	I_b
Supply of signal d_1	m_1	1	1	1	1
Switch	R_{on}	1	0	1	0
Diode	R_{on}	1	0	1	0
Coil	L	1	0	1	0
Coil	R_L	1	0	1	0
Capacitor	C	0	1	1	0
Load resistor	R	0	1	1	0
Sensor of i_L	i_L	1	1	1	0
Sensor of u_C	u_C	1	1	1	0

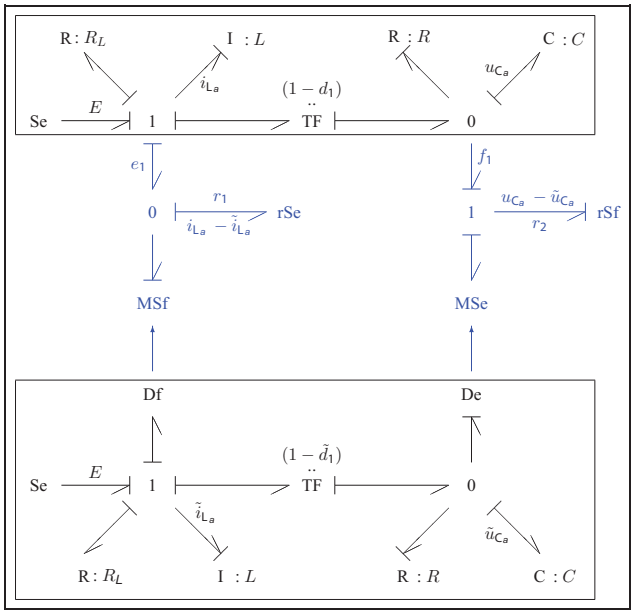

Figure 16. An averaged bond graph model representing the non-faulty boost converter behaviour (upper part) coupled to an averaged bond graph model accounting for a temporary fault in the duty ratio (lower part).

Figure 16. The mathematical model is a DAE system for the descriptor vector $x = (i_{L_a}, u_{C_a}, \tilde{i}_{L_a}, \tilde{u}_{C_a}, r_1, r_2)$. The residuals to be determined are components of the descriptor vector. In order to facilitate the numerical computation of the combined models, the residual sinks have been replaced by an artificial storage element–resistor pair that has no physical meaning.

Figure 17 displays the time evolution of the two averaged residuals r_1 and r_2. As can be seen, they deviate from zero during the time interval in which the duty ratio is equal to the lower value of 0.35 indicating a change in the duty ratio in accordance with the fault signature matrix. The simulation results can be verified by analytical computation of the residuals. Let $R_{on} \approx 0$. Reformulation of the ARR for r_1 yields

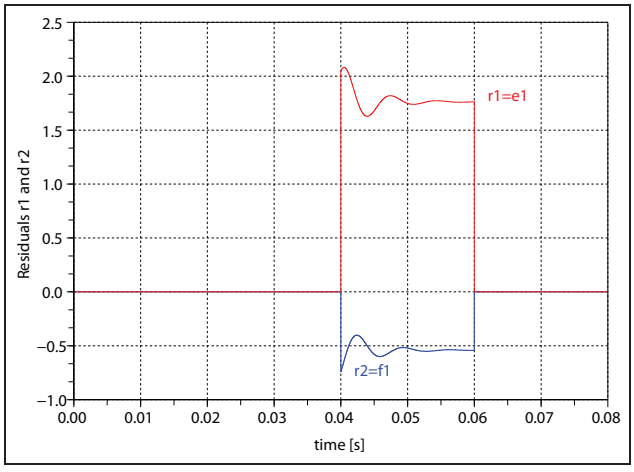

Figure 17. Time history of the averaged residuals r_1 and r_2 indicating a temporary fault in the duty ratio d_1.

$$r_1 = (1-d_1)u_{Ca} \underbrace{-R_L i_{La} - L\frac{di_{La}}{dt} + E}_{(1-\tilde{d}_1)u_{Ca}} \Bigg($$

$$r_1 = (d_1 - \tilde{d}_1)u_{Ca} \qquad (18)\leftarrow$$

Likewise, an expression for r_2 is obtained

$$r_2 = (\tilde{d}_1 - d_1)i_{La} \qquad (19)\leftarrow$$

According to equation (18), $-r_1(0.6) = (0.45 - 0.35) \times u_{Ca}(0.6) \approx 0.1 \times 17.5 = 1.75$ in agreement with Figures 14 and 17. Time history plots of the analytical expressions of the two residuals are the same as those obtained by simulation. Equations (18) and (19) indicate that in this case a set of ODEs is to be solved for some variables needed for the evaluation of additional unused equations. Svärd and Nyberg[41] present an algorithm that finds computation sequences for variables and residual equations in the general case of semi-explicit DAE systems.

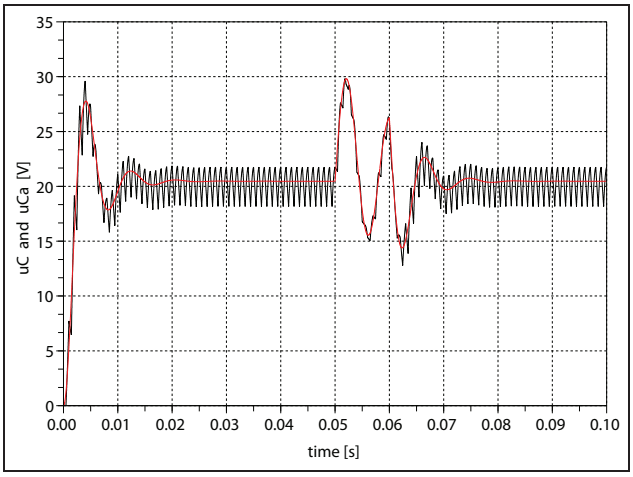

Figure 19. Time response of the capacitor voltage u_C to an increased value of the load resistance during the time interval [0.05 s, 0.06 s].

Fault scenario 2: temporary change of the load resistance R

Simulation of the system. As a second fault scenario, let the load resistance R jump at $t = 0.05$ s from 5.0Ω to 50.0Ω and stay at this value for 0.01 s. (If the boost converter is connected to a motor and if the angular velocity increases due to a decreased load torque then the induced voltage increases and the armature current decreases. If the boost converter's load is just modelled by an electrical resistor such a change can be taken into account by an increase of its resistance.) Figures 18 and 19 show the transient responses of the inductor current i_L and the voltage drop u_C across the capacitor as well as their averaged time evolution.

Numerical computation of ARRs. According to the ARRs derived from the diagnostic bond graph in Figure 15 or the FSM in Table 3, the change in the load resistance affects residual r_2 but not r_1. In fact, as can be seen from the numerically computed time evolution of the averaged residuals displayed in Figure 20, only residual r_2 deviates from zero during the time interval [0.05 s, 0.06 s]. The time response of r_2 obtained from a simulation of the faulty system model coupled to the non-faulty one can be checked in the following way. Residuals r_1 and r_2 fed into the non-faulty system model force this model to adapt to the disturbed behaviour of the faulty one. That is

$$C\frac{\tilde{u}_{C_a}}{dt} = (1-d_1)\tilde{i}_{L_a} - \frac{\tilde{u}_{C_a}}{R} - r_2 \qquad (20)\leftarrow$$

$$C\frac{\tilde{u}_{C_a}}{dt} = (1-d_1)\tilde{i}_{L_a} - \frac{\tilde{u}_{C_a}}{\tilde{R}} \qquad (21)\leftarrow$$

Hence

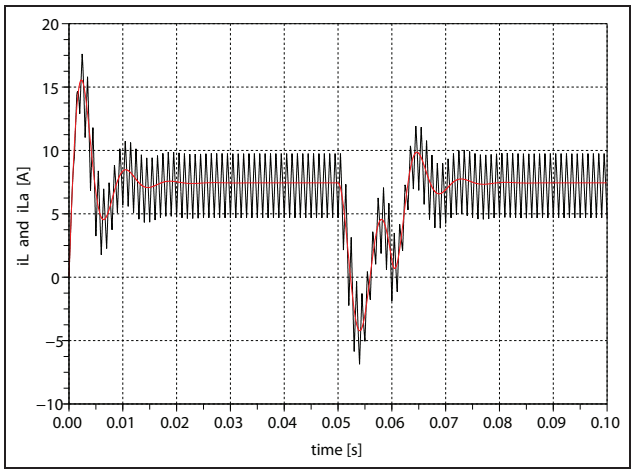

Figure 18. Time response of the inductor current i_L to an increased value of the load resistance during the time interval [0.05 s, 0.06 s].

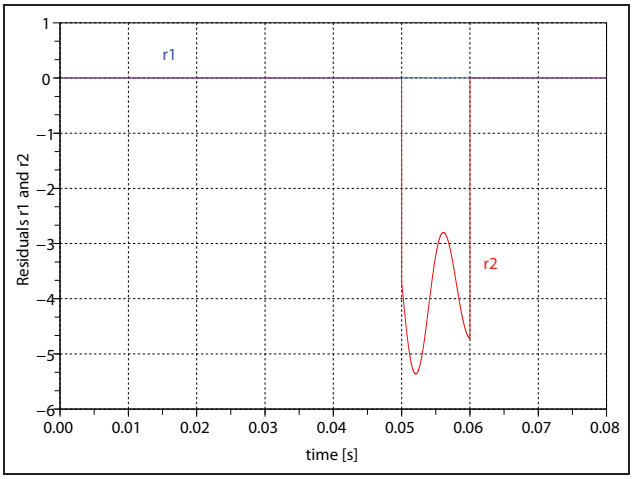

Figure 20. Time response of the averaged residuals r_1 and r_2 due to an increased value of the load resistance in the interval [0.05 s, 0.06 s].

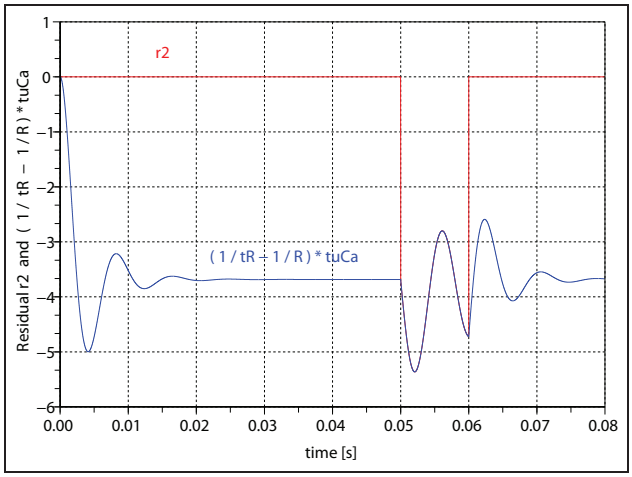

Figure 21. Plot of the averaged residual r_2 and the scaled averaged capacitor voltage versus time.

$$r_2 = \frac{1}{\tilde{R}} \quad \frac{1}{R} \quad \tilde{u}_{C_a} \qquad (22)$$

If the time response of $\tilde{u}_{C_a}$ obtained by simulation of the coupled models is scaled, then the plots of r_2 and the scaled capacitor voltage are actually identical in the interval [0.05 s, 0.06 s] as Figure 21 shows. In that figure, the tilde in equation (22) is indicated by the letter t. As can be seen from Figure 19, shortly after the abrupt change of the load resistor at $t = 0.05$ s, the capacitor voltage u_C takes the maximal value of 30 V. According to equation (22), $r_2 = (\quad 9/50) \times \tilde{u}_{C_a} = \quad 0.18 \times 30 = \quad 5.4$ A which is in agreement with Figure 21.

Structural observability and structural controllability of hybrid systems

Due to switches, the structure of hybrid system models is inherently time variant. System parts are temporarily disconnected while others are connected and vice versa. Hence, given a certain sensor placement and a set of signals controlling the system, structural observability and structural controllability of hybrid systems may be system mode dependent. However, faults can only be detected if the system is observable. Moreover, a control that is changed after a fault has happened is only applicable if the faulty system remains controllable. Therefore, it is essential to analyse a hybrid system with regard to structural observability and structural controllability.

For linear multiple-input multiple-output (MIMO) system models, structural observability and structural controllability can be directly checked on a bond graph with preferred integral causality. According to two theorems given by Sueur and Dauphin-Tanguy,[42] in essence, structural observability holds if there is a causal path from each storage element in integral causality to at least one sensor. The system is completely structurally input controllable if there is a causal path from a source to each storage element in integral causality. In hybrid system models, these paths may cross Boolean-controlled transformers representing switches. Depending on switch states, these causal paths may be cut off temporarily. This could be marked on the bond graph by highlighting the modulus of transformers representing switches in OFF mode in red colour or by crossing out the MTF.

The application of the two theorems to the previously considered boost converter model reveals that the system with the two sensors for the current i_L through the inductor and the voltage drop u_C across the load capacitor is structurally observable in all modes. This, however, does not necessarily mean that faults can be isolated. According to the structural FSM in Table 3 all faults can be detected but only a fault in the switching signal $m_1(t)$ can be isolated. This is not surprising, as a disturbance of the current i_L may be caused either by a faulty inductance L or a faulty resistance R_L. Likewise, if the measured time history of the voltage drop u_C deviates from normal operation, this may be due to either a faulty load capacitance C or a faulty load resistance R. The two elements are connected in parallel.

Furthermore, structural controllability does not hold in all system modes. Clearly, if the switch S_w is ON and the diode D is OFF, the voltage drop u_C across the load capacitor cannot be controlled by the voltage source Se : E.

Speed control of a buck converter driven DC-motor

In the second case study, the previously considered boost converter is replaced by a buck converter and the load resistor by a permanent magnet DC motor driving a torque load. Disturbances of its angular velocity are fed into a proportional–integral (PI) controller which controls the switch of the buck converter. By this way, the motor speed is controlled. A circuit schematic of this power electronic system is displayed in Figure 22. Figure 23 shows a bond graph of the buck converter. Again, the capacitor $C : C_a$ has been added to the junction 0_1 in order to resolve the causal conflict caused by the fixed conductance causality of the ON resistance of the switches. In

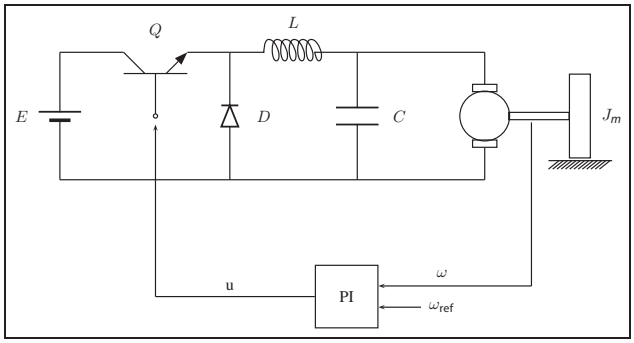

Figure 22. Buck-converter-driven DC motor.

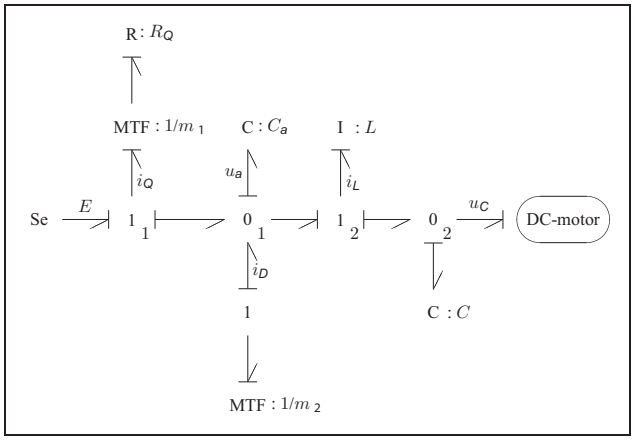

Figure 23. Bond graph model of the buck converter circuit.

the equations derived from the bond graph, the parameter C_a is set to zero. If the ON resistances of the switch and the diode are assumed equal ($R_Q = R_D = R_{\text{on}}$) the state equations derived from the bond graph of the buck converter in Figure 23 take a simpler form

$$\frac{di_L}{dt} = \frac{1}{L}[m_1 E \quad R_{\text{on}} i_L \quad u_C](\tag{23a}\leftarrow$$

$$\frac{du_C}{dt} = \frac{1}{c}\left[i_L \quad \frac{u_C}{R}\right]\Big(\tag{23b}\leftarrow$$

The buck converter can be represented by the simpler bond graph model in Figure 24 capturing the free wheel mode and the load mode. The buck converter bond graph in Figure 24 also represents an average model if the modulus m_1 is replaced by the duty ratio d.

Finally, Figure 25 shows an average bond graph model of the controlled buck-converter-driven DC motor. From the bond graph in Figure 25, the following state equations can be derived

$$\frac{d}{dt}\begin{bmatrix}\omega\\ i_a\\ u_C\\ i_L\end{bmatrix}\Big(= \begin{bmatrix}\frac{r}{J_m} & \frac{k}{J_m} & 0 & 0\\ \frac{k}{L_m} & \frac{R_m}{L_m} & \frac{1}{L_m} & 0\\ 0 & \frac{1}{C} & 0 & \frac{1}{C}\\ 0 & 0 & \frac{1}{L} & \frac{R_{\text{on}}}{L}\end{bmatrix}\begin{pmatrix}\omega\\ i_a\\ u_C\\ i_L\end{pmatrix}\Big(+ \begin{bmatrix}\frac{1}{J_m} & 0\\ 0 & 0\\ 0 & 0\\ 0 & \frac{1}{L}\end{bmatrix}\begin{pmatrix}T_{\text{load}}\\ uE\end{pmatrix} \tag{24}\leftarrow$$

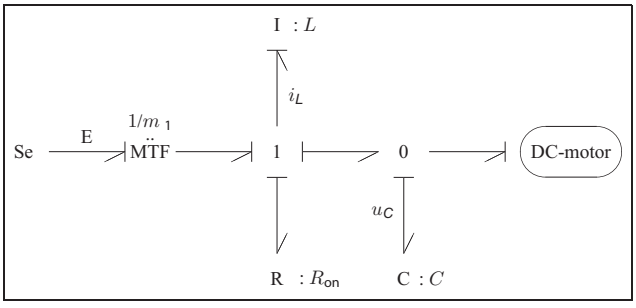

Figure 24. Simplified bond graph model of the buck converter circuit.

The PI controller equation reads

$$\dot{u} = k_p(\dot{e} + \frac{1}{T_i}e)$$

$$= k_p(\dot{\omega}_{\text{ref}} \quad \dot{\omega}) + \frac{k_p}{T_i}(\omega_{\text{ref}} \quad \omega) \tag{25}\leftarrow$$

where k_p denotes the proportional gain and T_i the integral time constant.

It is assumed that the inductor current i_L, the voltage drop across the capacitor u_C, the armature current i_a and the angular velocity ω of the motor are measured and, hence, are known quantities.

Figure 26 shows a DBG of the controlled buck-converter-driven DC motor. Adding efforts at the 1-junctions and flows at junction 0_1 in the diagnostic bond graph yields the following ARRs

$$1_1: \quad r_1 = uE \quad R_{\text{on}} i_L \quad L\frac{di_L}{dt} \quad u_C = [k_p(\omega_{\text{ref}} \quad \omega)$$

$$+ \frac{k_p}{T_i}\int_0^t (\omega_{\text{ref}} \quad \omega)d\tau \; E \quad R_{\text{on}} i_L \quad L\frac{di_L}{dt} \quad u_C \tag{26}$$

$$1_2: \quad r_2 = u_C \quad R_m i_a \quad L_m \frac{di_a}{dt} \quad k\omega \tag{27}$$

$$1_3: \quad r_3 = k i_a \quad r\omega \quad J_m\dot{\omega} \quad T_{\text{load}} \tag{28}$$

$$0_1: \quad r_4 = i_L \quad C\dot{u}_C \quad i_a \tag{29}$$

The controller equation provides the additional ARR

$$r_5 = \quad u + k_p(\omega_{\text{ref}} \quad \omega) + \frac{k_p}{T_i}\int_0^t (\omega_{\text{ref}} \quad \omega)d\tau \tag{30}$$

Table 4 displays the corresponding structural FSM. As in the previous example, it is assumed that the sensors are non-faulty. That is, their rows could be omitted.

Fault scenario 1: friction temporarily increases

Simulation of the system. The first fault scenario assumes that friction instantaneously triples at time instant $t = 1$ s and remains at that level for the period of 1 s. Let pulse(t,1.0,2.0) denote a pulse of height one between $t = 1$ s and $t = 2$ s and $\tilde{r}$ the disturbed friction coefficient. Then

$$\tilde{r}(t) = r + 2 \quad r \quad \text{pulse}(t, 1.0, 2.0) \tag{31}$$

The simulation run adopts the parameter values listed in Table 5. Figure 27 displays the time history of the averaged angular velocity due to the temporary increase of friction. At $t_1 = 1$ s, the averaged angular velocity drops to a value of about 33 rad/s. The PI controller forces the motor to regain the set value of 50 rad/s.

Numerical computation of ARRs. For numerical evaluation of the residuals, a bond graph model of the non-faulty system and a bond graph model of the system subject to disturbances are coupled by means of residual sinks as in the previous example. In this scenario, the bond

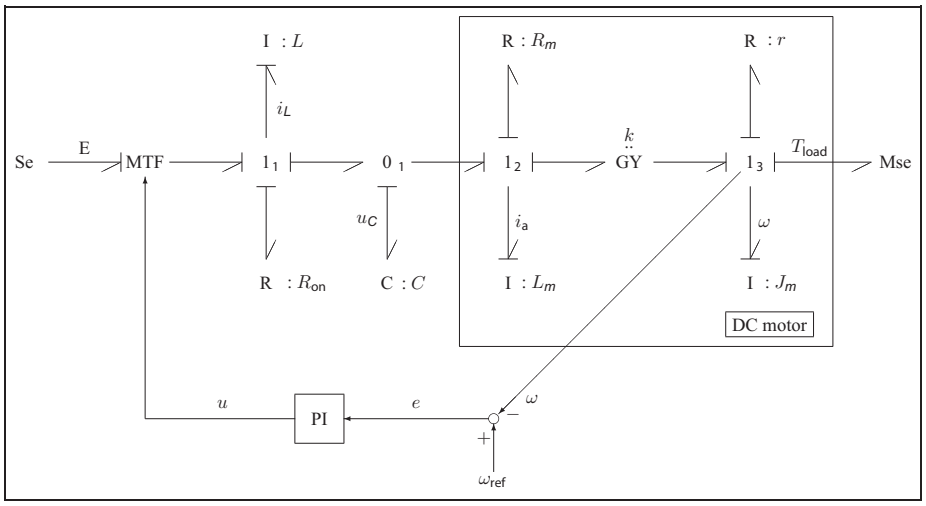

Figure 25. Bond graph model of the controlled buck-converter-driven DC motor.

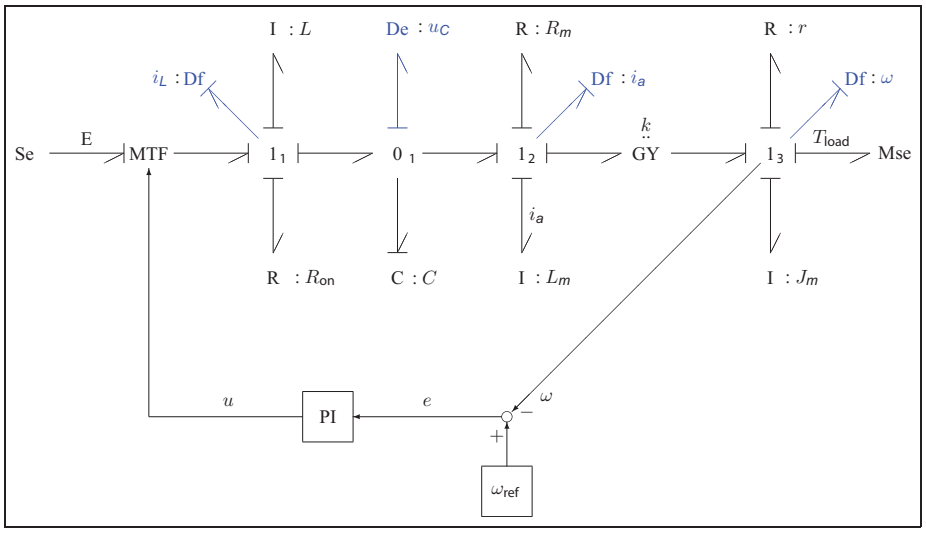

Figure 26. Diagnostic bond graph of the controlled buck-converter-driven DC motor.

Table 4. Structural FSM of the buck-converter-driven motor with sensors Df : i_L, De : u_C. De : i_a and De : ω.

Component	Parameter	r_1	r_2	r_3	r_4	r_5	D_b	I_b
PI controller	k_p, T_i	1	0	0	0	1	1	1
Buck converter inductance	L	1	0	0	0	0	1	1
Buck converter capacitor	C	1	0	0	1	0	1	1
Motor armature resistance	R_m	0	1	0	0	0	1	0
Motor armature inductance	L_m	0	1	0	0	0	1	0
Motor constant	k	0	1	1	0	0	1	1
Moment of inertia	J_m	0	0	1	0	0	1	0
Friction	r	0	0	1	0	0	1	0
Load moment	T_{load}	0	0	1	0	0	1	0
Sensor of i_L	i_L	1	0	1	1	0	1	1
Sensor of u_C	u_C	1	1	0	0	0	1	1
Sensor of i_a	i_a	0	1	0	1	0	1	1
Sensor of ω	ω	0	0	1	0	1	1	1

graph model of the faulty system accounts for a pulse in friction. Simulation of the coupled systems by means of the program Scilab[43] produces the time evolutions of the averaged residuals depicted in Figure 28. Residual r_3 clearly indicates the change in friction during the time interval from $t = 1$ s to $t = 2$ s, while residual r_1 is

Table 5. Parameters of the buck-converter-driven DC motor.

Parameter	Value	Units	Meaning
E	12.0	V	Voltage supply
L	20	mH	Inductance
R_{on}	0.1	Ω	ON resistance (switch, diode)
C	400	μF	Capacitance
L_m	2.6	mH	Armature inductance
R_m	2.0	Ω	Armature resistance
k	0.046	V s/rad	Motor constant
J_m	7.0 10 ^{5}	kg m^2	Moment of inertia
r	8.4 10 ^{4}	N m s/rad	Friction coefficient
T_{load}	0.05	N m	Load moment
k_p	0.0072	s/rad	PI controller's proportional gain
T_i	0.05	s	Integral time constant
ω_{ref}	50	rad/s	Reference speed

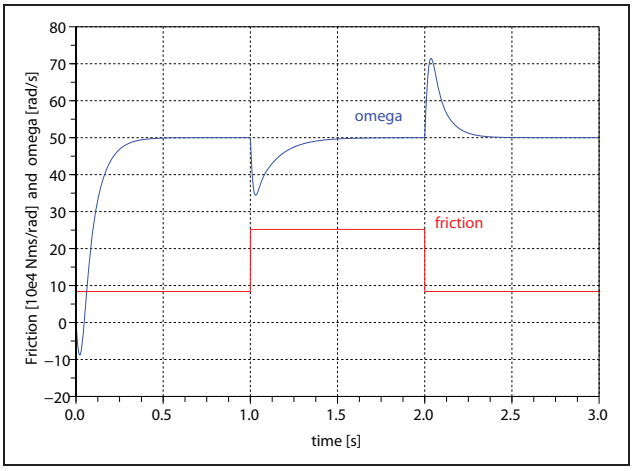

Figure 27. Time history of the averaged angular velocity due to a temporary change of friction.

not sensitive to this change as to be expected from the analytical expressions of the ARRs and their corresponding structural FSM in Table 4.

Figure 28 shows that residual r_3 reaches a value of about 0.081 Nm in the time interval 1 s $\leqslant t \leqslant$ 2 s. This can be analytically verified. Residual r_3 vanishes in case there is no disturbance at all. That is

$$0 = ki_a \quad r \quad \omega \quad J_m\dot{\omega} \quad T_{\text{load}} \tag{32}$$

and

$$\hat{r}_3 = ki_a \quad \tilde{r} \quad \omega \quad J_m\dot{\omega} \quad T_{\text{load}} \tag{33}$$

Hence

$$r_3 = -\hat{r}_3 = (\tilde{r} \quad r)\omega \tag{34}$$

In the time interval 1 s $\leqslant t \leqslant$ 2 s, the PI controller forces the angular velocity ω to rise to the value of 50 rad/s. According to (34) and (31) $r_3(t = 2.0\,\text{s}) = 2r \quad \omega =$

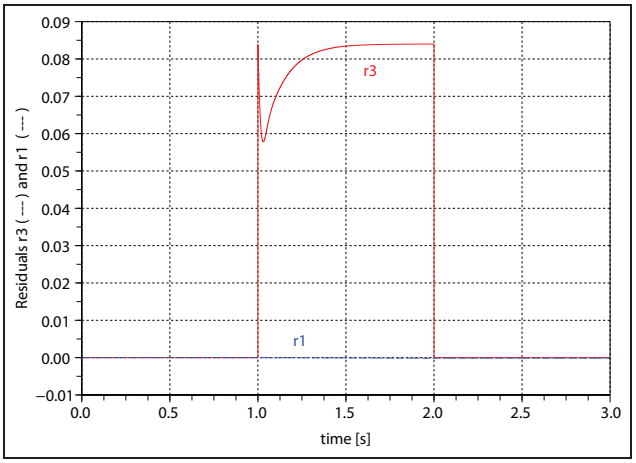

Figure 28. Time history of the averaged residuals r_1 and r_3.

2 8.4 10 ^{4} 50 = 0.084 [Nm] in accordance with Figure 28.

Fault scenario 2: the PI controller temporarily fails

In the second fault scenario, the PI controller is assumed to provide a faulty constant output of value zero for the time period 0.2 s $\leqslant t \leqslant$ 0.8 s as depicted in Figure 29. In the Scilab simulation of this scenario, the instantaneous mode changes of the controller from normal operation mode to faulty mode and vice versa is taken into account by a change between two sets of ordinary differential equations (ODEs) and a proper initialisation of the computation of the behaviour in each mode. At time $t_1 = 0.2$ s, the values of all state variables except the one for the controller output u are taken as initial values for the ODE set that holds for the time interval in which the controller fails. The initial value of u for the time interval [0.2 s, 0.8 s] is zero and the ODE for the controller reduces to $\dot{u} = 0$.

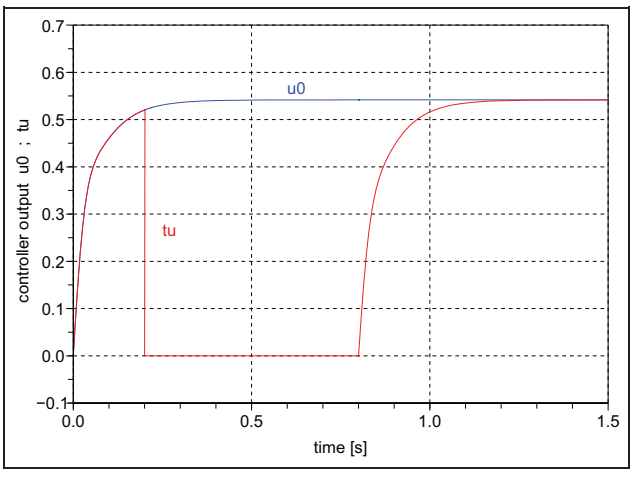

Figure 29. Controller output for the non-faulty case (u0) and the faulty case (tu).

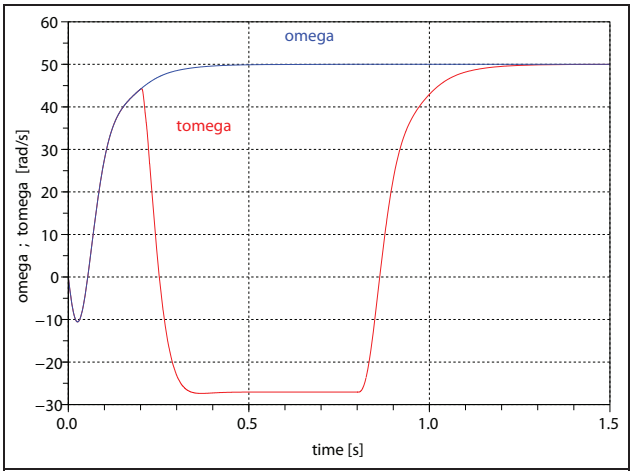

Figure 30. Time evolution of the angular velocity: omega: controller fully operational, tomega: controller temporarily out of order.

As can be seen from Figure 29, the controller output reaches the value 0.5417 which is the steady-state value that can be computed analytically.

Figure 30 shows the rise of the angular velocity to its reference value $\omega_{\text{ref}} = 50\,\text{rad/s}$ in the case that the PI controller is operating without interruption (omega) and in the case it is temporarily out of order (tomega = $\tilde{\omega}$). Analytical computation of the steady-state value of the angular velocity ω in the time interval [0.2 s, 0.8 s] yields

$$r + \frac{k^2}{R_m + R_{\text{on}}}\ \omega = \quad T_{\text{load}} \qquad (35)$$

As equation (35) shows, the negative steady-state value of ω in Figure 30 is due to the load torque. Inserting numerical values gives $\omega_s = \quad 27.06\,\text{rad/s}$ in agreement with the simulation results in Figure 30.

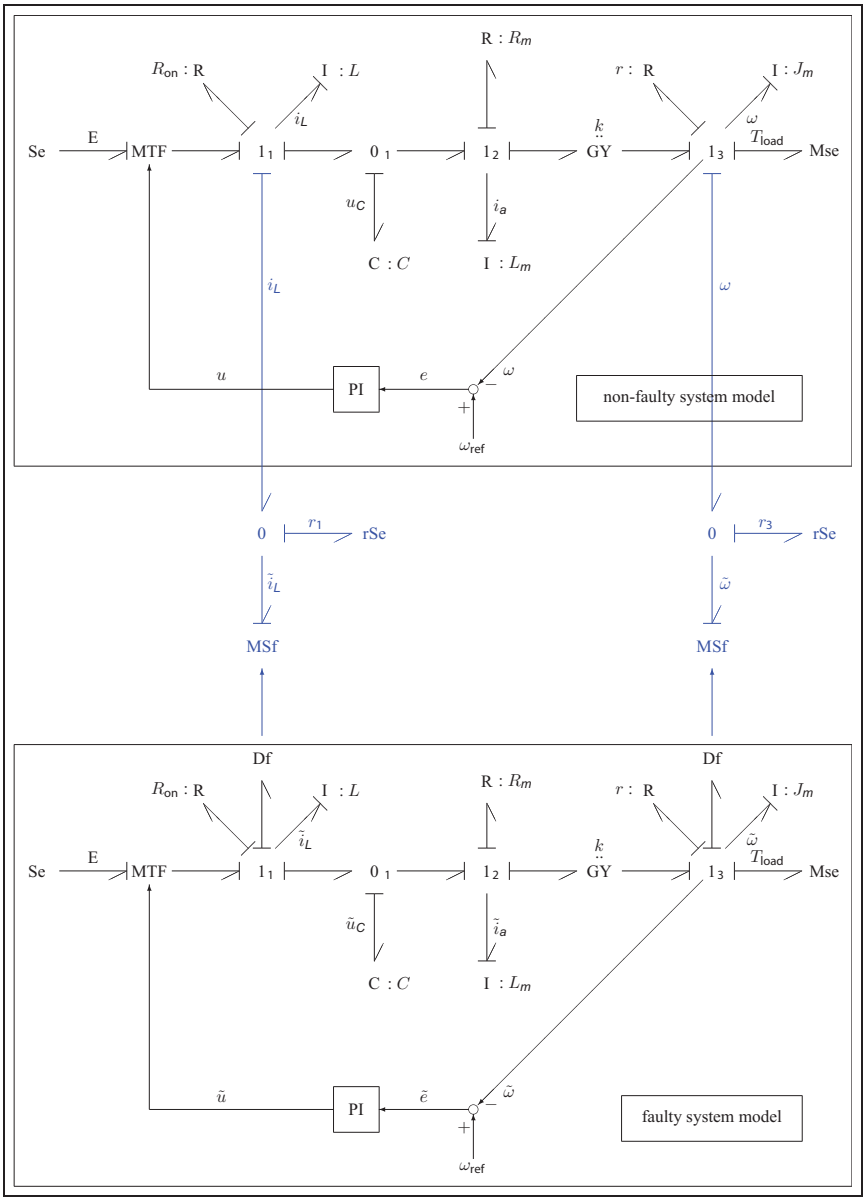

Figure 31. Non-faulty and faulty system model coupled by residual effort sinks.

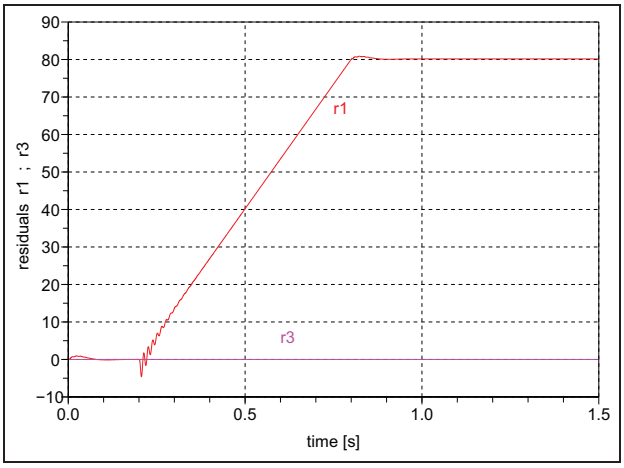

Figure 32. Time evolution of the residuals r_1 and r_3.

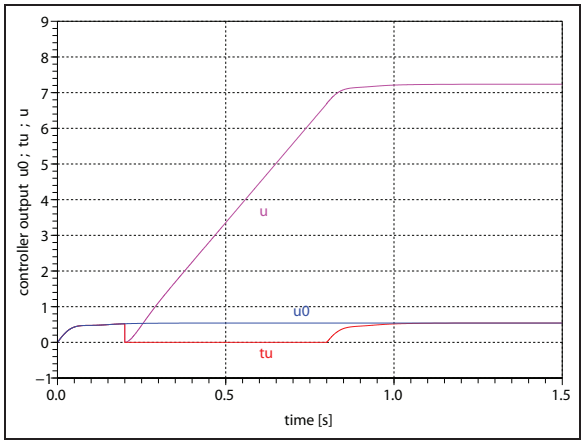

Figure 33. Time evolution of the controller output in the non-faulty system model coupled to the faulty system model.

According to the structural FSM (Table 4), the temporary failure of the PI controller affects the residuals r_1 and r_5 but not, for example, r_3. For the numerical computation of the residuals r_1 and r_3, the non-faulty model and the model subject to a temporary failure of the controller have been coupled by two residual effort sinks. Each of them imposes an effort onto the non-faulty system model so that it adapts its behaviour to the one of the faulty system (see Figure 31). Figure 32 confirms that residual r_1 is affected, while r_3 is not.

The simulation result for r_1 can be checked in the following manner. The residuals cause the non-faulty, perfectly controlled system to adapt its behaviour to the faulty one. That is, adding efforts at junction 1_1 in the non-faulty system model yields

$$uE = R_{\text{on}}\,\tilde{i}_L + \frac{d\tilde{i}_L}{dt} + \tilde{u}_C + r_1 \tag{36}$$

where the tilde denotes the faulty behaviour in time. For the model of the faulty system, summation at junction 1_1 gives

$$\tilde{u}E = R_{\text{on}}\,\tilde{i}_L + \frac{d\tilde{i}_L}{dt} + \tilde{u}_C \tag{37}$$

Hence

$$r_1 = (u \quad \tilde{u})E \tag{38}$$

Due to the temporary failure of the controller in the model of the faulty system for $0.2\,\text{s} \leqslant t \leqslant 0.8\,\text{s}$, the angular velocity $\tilde{\omega}$ remains constant during the time interval [0.4 s, 0.8 s] (Figure 30). As $\omega = \tilde{\omega}$, the equation of the controller in the model of the non-faulty system reduces to

$$\dot{u} = \frac{k_p}{T_i}(\omega_{\text{ref}} \quad \tilde{\omega}) \tag{39}$$

Inserting numerical values yields $\dot{u} = (0.0072/0.05)$ $(50 \quad (\quad 27.06)) = 11.096$. Hence

$$u(t = 0.8\,\text{s}) = 11.096 \quad 0.6 = 6.66 \tag{40}$$

and finally

$$r_1(t = 0.8\,\text{s}) = (6.66 \quad 0.0) \quad 12 = 79.9 \tag{41}$$

These values are in agreement with simulation results depicted in Figures 32 and 33. The latter figure shows the time evolution of the controller output u in the non-faulty system model coupled to the faulty system model. $u0$ denotes the output of the non-faulty controller in the case that the non-faulty system model is not coupled to the faulty one. A plot of $(u \quad \tilde{u})E$ versus time is identical to the one of r_1 obtained from numerical computation of the coupled models (see Figure 32).

Finally, the PI controller forces $\tilde{\omega}$ to reach the set value ω_{ref}. That is, $\dot{\tilde{\omega}} = 0$ for sufficient large time values. As a result, the state equations yield the steady-state value

$$\tilde{u} = \frac{1}{E}(R_{\text{on}}\tilde{i}_L + \tilde{u}_C) = \frac{1}{12}(0.1 \quad 2.0 + 6.3) = 0.5417 \tag{42}$$

in agreement with Figures 29 and 33.

Inserting the steady-state value $r_1(t > 0.8\,\text{s}) = 79.9$ into (38) finally gives

$$u = \frac{r_1}{E} + \tilde{u} = 79.9/12 + 0.5417 = 7.20 \tag{43}$$

which agrees with the steady-state value of u in Figure 33.

Conclusion

The subject of this paper is a fixed causality bond-graph-based approach to quantitative fault diagnosis of hybrid systems. To that end, it is proposed to pick up on a long known proposal to model switching devices by a transformer modulated by a Boolean variable and a resistor in fixed conductance causality accounting for its ON resistance. Bond graph representations of hybrid system models developed this way have been used so far mainly for the purpose of simulation. The paper demonstrates that this representation

can well constitute an approach to bond-graph-based quantitative FDI of hybrid models offering the following advantages.

- The standard SCAP can be applied to the bond graph without modifications. There is no need for a SCAP that is specialised for FDI.
- Computational causalities once assigned are independent of system modes. There is no need for partially adjusting causalities after a change from one system operation mode to another.
- Neither model equations nor ARRs need to be derived again after a discrete change of a system mode.
- Existing bond graph software such as SYMBOLS[27] may be used to generate a single set of ARRs. As these ARRs include Boolean variables, there is not one single structural FSM but a set. Detection and isolation of faults become system mode dependent. As to simulation, there is no need for a special software supporting variable computational causality.
- Derived model equations and ARRs may be reformulated symbolically so that the ON resistance of (some) switches may tend to zero turning the model of a switching device into an ideal switch.
- The presented causality-invariant bond graph approach to FDI has proven useful for power electronic systems but is not confined to such systems.

The conductance causality of the resistor in the switch model may lead to causal conflicts at some junctions and may require an auxiliary storage element with a small parameter value to be attached. However, in the derivation of equations from a diagnostic bond graph with storage elements in preferred derivative causality, the parameter of these auxiliary storage elements can be set to zero so that the additional storage elements will not lead to a set of stiff model equations with regard to simulation performed for a numerical evaluation of the residuals of ARRs. If it is decided to keep the small ON resistance of the switch model, i.e. switching devices are not represented by ideal switches, then small time constants may result.

Hybrid bond graphs with controlled junctions thus variable computational causalities have been used by Low et al.[25] along with a SCAP especially modified for FDI. It is shown that the invariant causality diagnostic bond graph approach in this paper can produce the same ARRs as given by Low et al.[24,25] Moreover, two case studies of switching systems from power electronics have demonstrated the practical usefulness of the approach. Numerical results obtained from simulation runs with Scilab[43] have been analytically checked, giving confidence in this approach.

Funding

This research received no specific grant from any funding agency in the public, commercial, or not-for-profit sectors.

Acknowledgement

This paper is a completely revised and significantly extended version of a paper entitled *Analytical Redundancy Relations from Bond Graphs of Hybrid System Models* presented at the 5th International Conference on Integrated Modelling and Analysis in Applied Control and Automation (IMAACA 2011), Rome, Italy, September 12–14, 2011.

References

1. Garcia-Gomez J. *Approche bond graph pour la modélisation des effets thermiques dans les composants de commutation en électronique de puissance*. Universite des Sciences et Technologies de Lille, France, 1997.
2. Ducreux JP, Dauphin-Tanguy G and Rombaut C. Bond graph modelling of commutation phenomena in power electronic circuits. In: *International conference on bond graph modeling, ICBGM'93, Proceedings of the 1993 Western simulation multiconference* (ed JJ Granda FE and Cellier), 1993, pp.132–136. SCS Publishing.
3. Dauphin-Tanguy G and Rombaut C. Why a unique causality in the elementary commutation cell bond graph model of a power electronics converter. In: *1993 IEEE international conference on systems, man and cybernetics 1*. 1993, pp.257–263.
4. Buisson J, Richard PY and Cormerais H. Ideal versus non-ideal approaches in bond graph modelling of switching devices: a comparison based on singular perturbation theory. In: *Proceedings of the 4th international confrence on automation of mixed processes: hybrid dynamic systems (ADPM 2000)*, 2000, pp.257–264.
5. Borutzky W. Representing discontinuities by means of sinks of fixed causality. In: *1995 International conference on bond graph modeling, ICBGM'95, Proceedings of the 1995 Western simulation multiconference* (ed JJ Granda FE and Cellier), 1995, pp.65–72. SCS Publishing.
6. Borutzky W, Broenink JF and Wijbrans KCJ. Graphical description of physical system models containing discontinuities. In: *Modelling and simulation 1993, Proceedings of the 1993 European simulation multiconference*. (ed A Pave), Lyon, France, 1993, pp.208–214. SCS Publishing.
7. Umarikar AC. *Modelling of switched mode power converters: a bond graph approach*. Centre for Electronics Design and Technology, Indian Institute of Science, Bangalore, India, 2006.
8. Umarikar AC and Umanand L. Modelling of switched systems in bond graphs using the concept of switched power junctions. *J Franklin Inst* 2005; 342: 131–147.
9. Buisson J, Cormerais H and Richard PY. Analysis of the bond graph model of hybrid physical systems with ideal switches. *Proc IMechE, Part I: Systems and Control Engineering* 2002; 216: 47–63.
10. Edstrom K. *Switched bond graphs: simulation and analysis*. Linkoping University. Linkoping, Sweden, 1999.
11. Stromberg JE. *A mode switching modelling philosophy*. Linkoping University. Linkoping, Sweden, 1994.
12. Asher GM. The robust modelling of variable topology circuits using bond graphs. In: *International conference on bond graph modeling, ICBGM'93, Proceedings of the 1993 Western simulation multiconference* (ed JJ Granda and FE Cellier), 1993, pp.126–131. SCS Publishing.

13. Roychoudhury I, Daigle M, Biswas G, et al. A method for efficient simulation of hybrid bond graphs. In: *Proceedings of the 2007 international conference on bond graph modeling and simulation 39* (ed JJ Granda and FE Cellier), 2007, pp.177–184.
14. Mosterman PJ. *Hybrid dynamic systems: a hybrid bond graph modeling paradigm and its application in diagnosis*. Vanderbilt University, Nashville, TN, 1997.
15. Borutzky W. *Bond graph methodology – development and analysis of multidisciplinay dynamic system models*. London: Springer, 2010.
16. Tagina M, Cassar JP, Dauphin-Tanguy G, et al. Monitoring of systems modelled by bond-graphs. In: *ICBGM'95, International conference on bond graph modeling and simulation* (ed JJ Granda and FE Cellier). Las Vegas, NV, 1995, pp.275–280. SCS Publishing.
17. Borutzky W (ed). *Bond graph modelling of engineering systems – theory, applications and software support*. New York: Springer, 2011.
18. Borutzky W. Bond graph model-based fault detection using residual sinks. *Proc IMechE, Part I: Systems and Control Engineering* 2009; 223: 337–352.
19. Samantaray AK and Ould Bouamama B. *Model-based process supervision – a bond graph approach*. Advances in Industrial Control. London: Springer, 2008.
20. Djeziri MA, Merzouki R, Ould Bouamama B, et al. Robust fault diagnosis by using bond graph approach. *IEEE/ASME Trans Mechatron* 2007; 12: 599–611.
21. Ghoshal SK. *Model-based fault diagnosis and accommodation using analytical redundancy: a bond graph approach*. Department of Mechanical Engineering, Indian Institute of Technology, Kharagpur, India, 2006.
22. Samantaray AK, Medjaher K, Ould Bouamama B, et al. Diagnostic bond graphs for online fault detection and isolation. *Simul Modell Pract Theor* 2006; 14: 237–262.
23. Narasimhan S. *Model-based diagnosis of hybrid systems*. Vanderbilt University, 2002.
24. Low CB, Wang D, Arogeti S, et al. Causality assignment and model approximation for hybrid bond graph: fault diagnosis perspectives. *IEEE Trans Autom Sci Eng* 2010; 7: 570–580.
25. Low CB, Wang D, Arogeti S, et al. Monitoring ability analysis and qualitative fault diagnosis using hybrid bond graph. In: *Proceedings of the 17th world congress of the international federation of automatic control*, Seoul, Korea, 2008, pp.10516–10521.
26. Low CB, Wang D, Arogeti S, et al. Causality assignment and model approximation for quantitative hybrid bond graph-based fault diagnosis. In: *Proceedings of the 17th world congress of the international federation of automatic control*, Seoul, Korea, 2008. pp.10522–10527.
27. HighTec Consultants. SYMBOLS Shakti™. http://www.htcinfo.com/.
28. Bouamama BO, Samantaray AK, Staroswiecki M, et al. Derivation of constraint relations from bond graph models for fault detection and isolation. In: *Proceedings of the international conference on bond graph modeling, ICBGM'03* (ed JJ Granda and FE Cellier), Orlando, FL, 2003, pp.104–109. SCS Publishing.
29. Samantaray AK and Ghoshal SK. Sensitivity bond graph approach to multiple fault isolation through parameter estimation. *Proc IMechE, Part I: Systems and Control Engineering* 2007; 221: 577–587.
30. Borutzky W. Fault indicators and adaptive thresholds from hybrid system models. In: *7th Vienna international conference on mathematical modelling*, 2012.
31. Borutzky W and Granda JJ. Bond graph based frequency domain sensitivity analysis of multidisciplinary systems. *Proc IMechE, Part I: Systems and Control Engineering* 2002; 216: 85–99.
32. Patton RJ and Chen J. Design methods for robust fault diagnosis. In: *Control systems, robotics and automation* (ed H Unbehauen). Encyclopedia of life support systems (EOLSS), Eolss Publishers, Oxford, UK, 2009, vol. XVI, pp.84–111, http://www.eolss.net.
33. Gertler J. Fault detection and diagnosis in engineering systems. New York: Dekker, 1998.
34. Kam CS and Dauphin-Tanguy G. Bond graph models of structured parameter uncertainties. *J Franklin Inst* 2005; 342: 379–399.
35. Touati Y, Merzouki R and Ould Bouamama B. Fault detection and isolation in presence of input and output uncertainties using bond graph approach. In: *Proceedings of the 5th international conference on integrated modeling and analysis in applied control and automation (IMAACA 2011)* (ed. A Bruzzone, G Dauphin-Tanguy, S Junco and MA Piera), 2011, pp.221–227.
36. Basseville M and Nikiforov IV. *Detection of abrupt changes – theory and application*. Englewood Cliffs, NJ: Prentice-Hall, 1993. http://www.irisa.fr/sisthem/michele/.
37. Roychoudhury I, Daigle MJ, Biswas G, et al. Efficient simulation of hybrid systems: A hybrid bond graph approach. *Simulation*. 2011; 87: 467–498.
38. Roychoudhury I, Daigle M, Biswas G, et al. Efficient simulation of hybrid systems: an application to electrical power distribution systems. In: *Proceedings of the 22nd European conference on modelling and simulation (ECMS 2008)*, 2008, pp.471–477.
39. Allard B, Morel H, Lautier P, et al. Bond graphs for averaged modeling of power electronic converters. In: *Proceedings of the 1997 international conference on bond graph modeling and simulation* (ed JJ Granda and G Dauphin-Tanguy). 1997, pp.201–206. SCS Publishing.
40. Garcia-Gomez J, Dauphin-Tanguy G and Rombaut C. Average bond graph models of DC/DC power converters. In: *Proceedings of the 1999 international conference on bond graph modeling and simulation* (ed JJ Granda and FE Cellier), 1999, pp.338–343. SCS Publishing.
41. Svard C and Nyberg M. Residual generators for fault diagnosis using computation sequences with mixed causality applied to automotive systems. *IEEE Trans Syst Man Cybernet – Part A: Syst Humans* 2010; 40: 1310–1328.
42. Sueur C and Dauphin-Tanguy G. Bond-graph approach for structural analysis of MIMO linear systems. *J Franklin Inst* 1991; 328: 55–70.
43. Scilab Consortium. *Scilab*. http://www.scilab.org/.

Appendix

Notation

A	cross sectional area of a tank
C	capacitance
D	diode
d	duty ratio

Df	flow detector
De	effort detector
E	voltage supply
e	effort variable
f	flow variable
J	moment of inertia
k	motor constant
k_p	proportional coefficient of a PI controller
L	self-inductance
m	transformer modulus $m \in \{0, 1\}\leftarrow$
Q	volume flow rate
Q_p	pump outflow
p	pressure
R	resistance
r_i	residual i
r	friction coefficient
R_{on}	resistance of a switch in ON-mode
Sw	switch
T_i	integral time constant of a PI controller
T_s	switching time period
t	time
u	controller output
V	voltage
ω	angular velocity
ρ	fluid density (assumed constant)